Biophysical Chemistry 136 (2008) 115–123

Contents lists available at ScienceDirect

Biophysical Chemistry

journal homepage: http://www.elsevier.com/locate/biophyschem

Solution ^{1}H NMR study of the active site structure for the double mutant H64Q/V68F cyanide complex from mouse neuroglobin

Guowei Yin [a,1], Yanjie Li [b,1], Juan Li [c], Jing Li [b], Weihong Du [a,*], Qun Wei [b,*], Weihai Fang [c]

[a] Department of Chemistry, Renmin University of China, Beijing 100872, China
[b] Department of Biochemistry and Molecular Biology, Beijing Normal University, Beijing 100875, China
[c] College of Chemistry, Beijing Normal University, Beijing 100875, China

ARTICLE INFO

Article history:
Received 3 April 2008
Received in revised form 12 May 2008
Accepted 12 May 2008
Available online 19 May 2008

Keywords:
Mouse neuroglobin
Double mutant
Cyanide complex
NMR
Solution structure

ABSTRACT

Solution ^{1}H NMR spectroscopy has been carried out to investigate the molecular and electronic structures of the active site in H64Q/V68F double mutant mouse neuroglobin in the cyanomet form. Two heme orientations resulting from a 180° rotation about the α–γ-meso axis were observed with a population ratio about 1:1, and the clearly distinguished B isomer was used to perform the study. Based on the analysis of the dipolar shifts and paramagnetic relaxation constants, the distal Gln^{64}(E7) side chain is obtained to adopt an orientation that may produce hydrogen bond between the $N_{\varepsilon}H_1$ and the Fe-bound cyanide. The side chain of Phe^{68}(E11) is oriented out of the heme pocket just like that in triple mutant of cyanide complex of sperm whale myoglobin. A 15° rotation of the imidazole ring in axial His^{96} is observed, which is close to the ϕ angle determined from the crystal structure of NgbCO. The quantitative determinations of the orientation and anisotropies of the paramagnetic susceptibility tensor reveal that cyanide is tilted by 8° from the heme normal which allows for contact to the Gln^{64}(E7) $N_{\varepsilon}H_1$. The E7 and E11 residues appear to control the direction and the extent of tilt of the bound ligand. Furthermore, the tilt of the ligand has no obvious influence on the heme heterogeneity of cyanide ligation for isomer A/B of the wild type and mutant protein, indicating that factors other than steric effects, such as polarity of heme pocket, impacts on ligand binding affinity.

1. Introduction

Neuroglobin (Ngb) [1,2] is a newly discovered hemoprotein, found in the brain of fishes, amphibians and birds, and is likely present in the nervous system of all vertebrates [3]. From amino acid sequence, Ngb is distantly related to hemoglobin (Hb) and myoglobin (Mb), with only about 25% sequence identity including some key amino acid residues, such as the histidines at position E7 and F8 which are highly conserved within the vertebrate globins [4]. Interestingly, based on sequence analysis, Ngb is more ancient than Mb. Although the physiological roles of Ngb are poorly understood, its low expression level *in vivo*, and its hexacoordination are indicative of functions other than temporary oxygen storage and/or a scavenger of bioactive compounds in hypoxic cells (i.e., NO, peroxynitrite, and hydrogen peroxide) [5–7].

From the crystal structure, unligated Ngb consists of eight α-helices and exhibits the typical globin "three-over-three α-helical sandwich" fold. As in the case of Mb and Hb, the proximal F8, histidyl imidazole (His^{96} in Ngb) coordinates to the heme iron as a fifth axial ligand. In the absence of an exogenous ligand, the distal histidine E7 of Ngb binds to the heme iron both in the ferric and ferrous states [8–12]; this feature was previously reported only for invertebrate [13,14] and plant globins [15]. Though another hexacoordinated vertebrate hemoprotein, Cytoglobin(Cgb), was reported recently [16,17], the two hexacoordinated globins still have huge difference in their structural heterogeneity, ligand binding affinity, heme cavity properties and physiological functions [17–19].

Ngb exhibits rapid recombination rate ($k_{on}(O_2)=300\times10^6$ M^{-1} s^{-1}) and slow dissociation rate ($k_{off}(O_2)=0.4$ s^{-1}) for both O_2 and CO [5–7]. The *in vivo* binding of exogenous ligands to ferrous Ngb show to break the distal bond with His^{64}(E7). The observed slow k_{off} rates for O_2 and CO are due to the strong stabilization of the ligand by His^{64}(E7). In contrast, globins that lack the His^{64}(E7) residue, e.g., Aplysia Mb, are found to have k_{on} rates which are similar to those of mammalian Mbs, while the observed k_{off} rates are much faster [20]. Thus, it has been suggested that His^{64}(E7) plays a key role in the stabilization of exogenous ligand binding, and also induces ligand rebinding [21].

Beyond the atypical kinetic features, it has been demonstrated from NMR studies by La Mar et al. that in solution the wild type cyanide complex of neuroglobin (WT-NgbCN) exhibits an unusual structural heterogeneity (Fig. 1) [22]. Furthermore, from recent crystal structures of Ngb and NgbCO [23–25] the presence of a large internal cavity has been

Abbreviations:, Ngb, neuroglobin, metNgbCN, cyanide ligated ferric neuroglobin, Mb, myoglobin, SWMb, sperm whale myoglobin, Hb, hemoglobin, WT, wild type, dm-metNgbCN, cyanide complex of double mutant neuroglobin in ferric form, Cytoglobin, Cgb, DSS, 2,2-dimethyl-2-silapentane-5-sulfonate, WEFT, water-eliminated Fourier transform, NOESY, two-dimensional nuclear Overhauser spectroscopy, TOCSY, two-dimensional total correlation spectroscopy.

* Corresponding authors. Tel.: +86 10 62512660; fax: +86 10 62516444.
E-mail addresses: whdu@chem.ruc.edu.cn (W. Du), weiq@bnu.edu.cn (Q. Wei).
[1] These authors contribute equally to this paper.

0301-4622/$ – see front matter © 2008 Elsevier B.V. All rights reserved.
doi:10.1016/j.bpc.2008.05.003

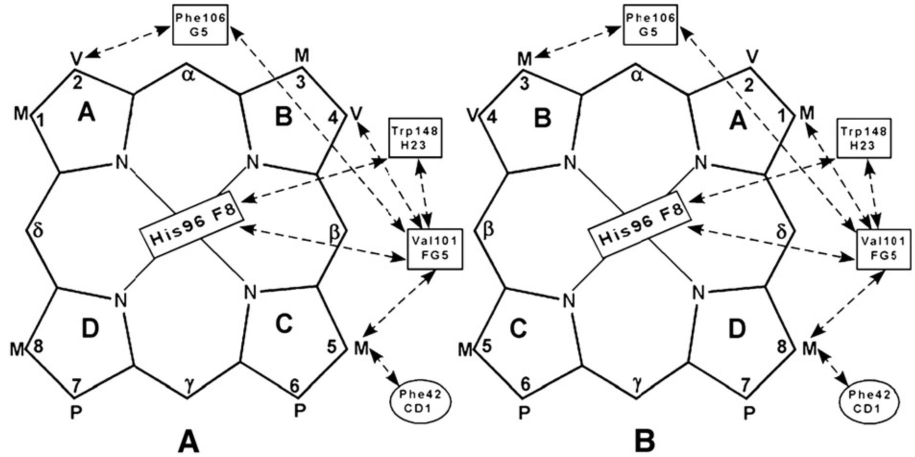

Fig. 1. Schematic representation of the heme pocket structure of dm-cyanometNgb with face-on view from the proximal side. The hemin substituents are labeled M(methyl), V(vinyl), and P(propionate). (A) isomer A, the same heme orientation as in SWMb. (B) isomer B, the heme orientation 180° rotated with respect to the α–γ-meso axis.

identified. By comparing the ligated and non-ligated crystal structures, CO binding induces a large sliding of the heme toward the interior of the protein and an extensive reorganization of the internal cavity. The external wall of the cavity is restricted by the EF loop, which was found to have unusual mobility like the CD loop [24]. Another quite peculiar characteristic of the Ngb heme pocket is the crowd of apolar residues (Val^{68}(E11), Phe^{42}(CD1) and Phe^{28}(B10)), particularly on heme distal side. This highly hydrophobic distal side is connected with two small cavities, one of which topologically corresponds to the so-called Xe4 cavity in sperm whale myoglobin(SWMb) [26]. The specific distal structure has prompted investigations of heme distal mutation and protein–protein interactions [27–31]. Based on important experimental evidence for vertebrate proteins [27,28,32–35], such as Hb, Mb and Cgb, proposed to be the closest cousins to the Ngb family, and as a paradigm for investigating the interaction of proteins and small molecule ligand, two residues, E7 and E11, located on the E-helix in the distal region of heme pocket, have been genetically engineered into various mutants, such as His64Gln, Val68Ala etc. These mutants are associated and retain the structural significance of the globin family.

For the E7 location, the proton donation capabilities of the Gln mutant are similar to that of the WT His residue. However, the flexibility and two proton donation capabilities of the Gln side chain can probe the conformation of the ligand. In contrast, the WT His has limited flexibility and only one proton donor site. On the distal side of heme for a variety of Mb system, the terminal hydrogen atoms of the E7 side chain are very likely to form hydrogen bond with the sixth ligand, and hence substantially stabilize the presence of the ligand [32]. In contrast, the substitution of Val for His has been reported to cause a significant decrease of the binding constant as the Val lacks the hydrogen bonding capacity [33]. Paralleling the manipulation above, the Val residue at the 11th site in the E-helix has been replaced by a Phe, in an attempt to modulate the strength and spatial orientation of the coordination bond

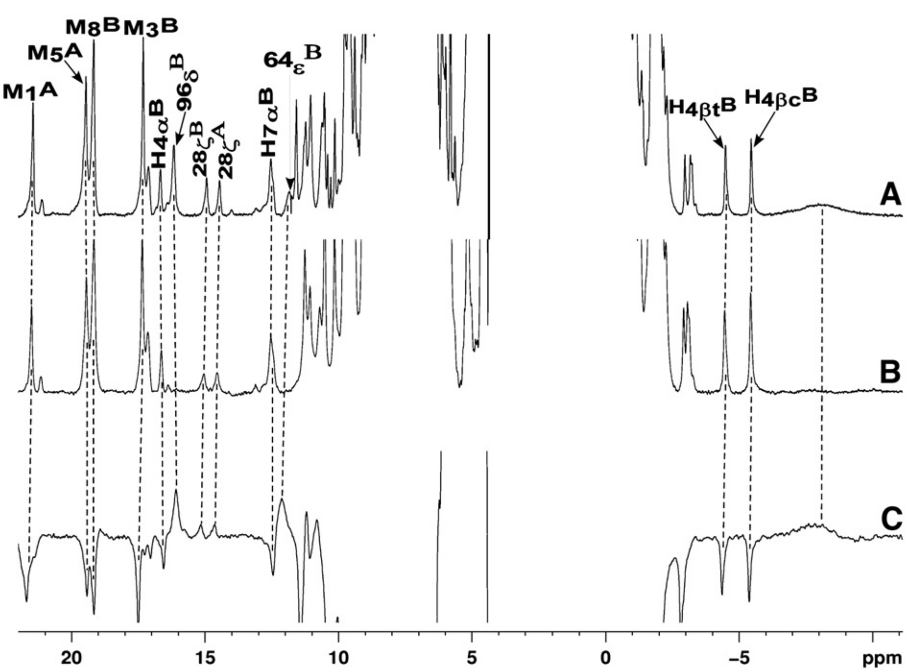

Fig. 2. 600 MHz ^{1}H NMR spectra of dm-cyanometNgbCN at 300 K, pH 7.5, 100 mM phosphate buffer. (A) Relaxed (repetition rate 1 s^{-1}) reference trace in ^1H_2O; (B) relaxed, reference trace in ^2H_2O; (C) WEFT spectrum(relaxation delay 30 ms, repetition rate 10 s^{-1}) in ^1H_2O which allows detection of strongly relaxed, broad signs at 11.77 and −7.12 ppm. Heme resonances are labeled as shown in Fig. 1, and residues are labeled by position numbers and protons.

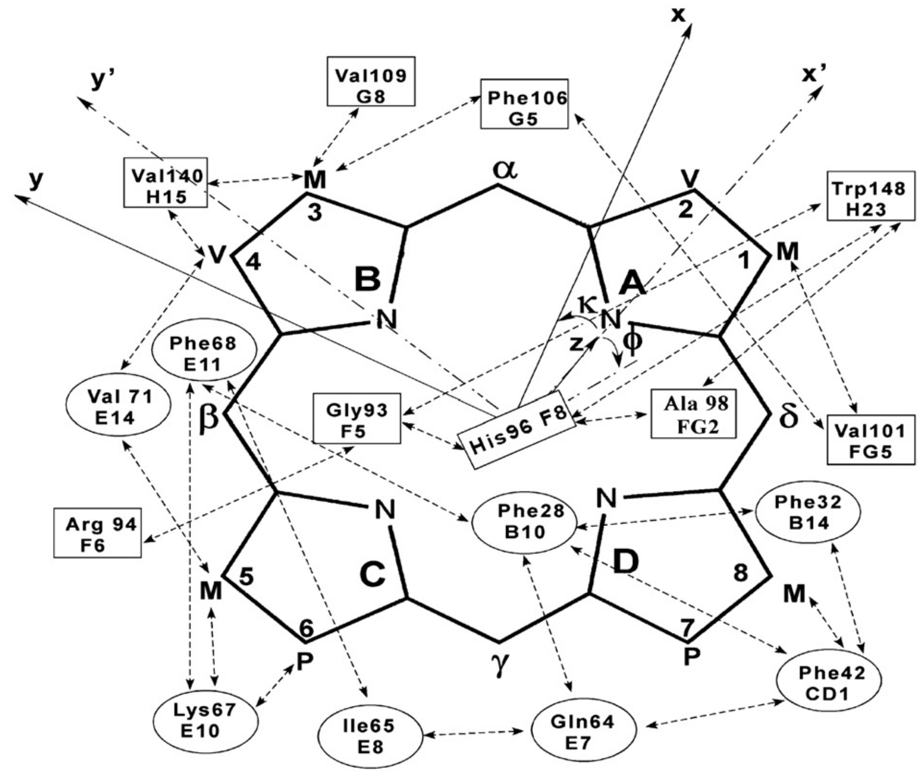

Fig. 3. Heme pocket structure in isomer B. Proximal and distal residues are represented as square and circles respectively. The double-sided arrows represent inter-residue and residue-heme dipolar contacts observed in dm-metMbCN. Also shown is the definition of the magnetic axes x, y, z relative to the iron-centered crystal coordinates x', y', z'. The two coordinate systems are related by the standard Euler rotation $\Gamma(\alpha, \beta, \gamma)$, where $[x, y, z] = [x', y', z']\,\Gamma(\alpha, \beta, \gamma)$. The tilt of the major magnetic or z axis from the heme normal is given by β, where α is the angle between the projection of the z axis tilt on the heme plane and the x' axis. In this case, $\alpha \sim 0°$.

in the active cavity via the restricted side chain motion at E11 [28]. A compelling illustration for this is the aquomet *Lucina* HbI, with Gln at E7 position and Phe at E11 [34].

As mentioned above, the residues from E-helix play important roles on ligand binding, heme cavity property and distal hydrogen bond network to affect the structure and function of neuroglobin [21–23]. Among them, the distal residue E7 (at the sixth ligand location) and E11 (at hydrophobic region) are quite specific. In order to understand the action of distal residues of E-helix on active sites of neuroglobin, we have adopted the strategy of site-directed mutagenesis at E7 and E11 sites to construct H64Q-V68F double mutant of mouse Ngb and to investigate the solution structure of cyanide complex of this mutant. Cyanide binds to the ferric state, and the resulting complex is a low-spin species readily studied by nuclear magnetic resonance spectroscopy at atomic and electronic level. The ^{1}H NMR spectra of mouse dm-Ngb cyanomet complex showed that two heme orientations resulting from a 180° rotation about the α–γ-meso axis were observed with a population ratio about 1:1(Fig. 2), and the clearly distinguished B isomer was used to perform the study. It will probe the "uncommon" inner cavity around the heme distal side of Ngb due to double mutations, and consequently lead to a detailed understanding of ligand binding and potential physiological mechanism.

2. Materials and methods

2.1. Protein sample

The double mutant H64Q/V68F neuroglobin (dm-Ngb) from mouse was expressed and purified as described previously [36]. Hemin was titrated into a solution of dm-Ngb apoprotein to a 1:1 stoichiometry in the presence of a 10 fold molar excess of KCN in a 90/10 $^1H_2O/^2H_2O$ solution buffered at pH 7.5 with 100 mM phosphate. The final concentration of mouse cyanomet-dmNgb complex (dm-metNgbCN) was about 2 mM. Deuterium exchange was subsequently performed using an Amicon ultrafiltration cell. Solution pH (not compensated for ^{2}H activity) was adjusted with NaO^{1}H (NaO^{2}H) or ^{1}HCl (^{2}HCl) solution. The sample was stored at 4°. Based on the reproducibility of 2D ^{1}H NMR spectra, the sample remained stable for longer than one year.

Table 1
^{1}H NMR spectral parameters for heme and His^{96}(F8) signals in mouse dm-metNgbCN

Residues	Proton	A	B
Heme	1-CH_3	21.05(115)	7.41
	3-CH_3		16.99 (150)
	5-CH_3	19.01 (112)	9.64
	8-CH_3		18.73 (126)
	2-H_α	16.81	
	2-$H_{\beta c}$	−1.49 (199)	
	2-$H_{\beta t}$	−2.24 (195)	
	4-H_α	7.54	16.36 (148)
	4-$H_{\beta c}$		−4.58 (217)
	4-$H_{\beta t}$		−3.67 (196)
	6-H_α	12.36	6.35
	6-$H_{\alpha'}$	9.78	2.12
	6-H_β		−1.37
	6-$H_{\beta'}$	0.30	−0.71
	7-H_α		12.45 (130)
	7-$H_{\alpha'}$		11.3
	7-H_β		0.06
	7-$H_{\beta'}$		0.27
His^{96}(F8)	NH	11.05	11.22
	$C_\alpha H$	8.08	8.48
	$C_\beta H$		9.01
	$C_{\beta'} H$		10.63
	$N_\delta H$	15.88 (34)	15.84 (34)

Chemical shifts in ppm are referenced to DSS in ^1H_2O 100 mM phosphate, pH 7.5, 300 K. Non-selective T_1, in ms, in parentheses for resolved resonances.

Table 2
^{1}H NMR spectral parameters for strongly dipolar shifted active site residues in mouse dm-metNgbCN isomer B

Residue	Proton	δ_{DDS} (obs)	δ_{DDS} (dia)	Residue	Proton	δ_{DDS} (obs)	δ_{DDS} (dia)
Phe^{28}(B10)	$C_\delta H$	8.21	6.37		$C_\alpha H$	4.61	3.22
	$C_\varepsilon H$	9.85	5.81	Gly^{93}(F5)	NH	10.2	7.48
	$C_\zeta H$	14.73 (49)	4.43		$C_\alpha H$	6.32	3.50
Phe^{32}(B14)	$C_\delta H$	6.96	7.21		$C_{\alpha'} H$	5.77	2.73
	$C_\varepsilon H$	7.08	7.17	Arg^{94}(F6)	NH	9.25	7.85
	$C_\zeta H$	7.63	6.83		$C_\alpha H$	4.61	4.01
Phe^{42}(CD1)	$C_\delta H$	6.50	7.55	Lys^{95}(F7)	NH	8.96	7.14
	$C_\varepsilon H$	7.37	6.85		$C_\alpha H$	4.96	3.36
Gln^{64}(E7)	$C_\beta H$	6.78	2.37		$C_\beta H$	3.04	1.42
	$C_\gamma H$	7.67	1.94		$C_{\beta'} H$	2.91	0.90
	$C_{\gamma'} H$	11.05	0.74	Arg^{97}(F9)	NH	9.84	6.21
	$N_\varepsilon H$	11.77 (22)	7.03		$C_\alpha H$	4.63	2.96
Ile^{65}(E8)	$C_\alpha H$	5.94	2.64	Ala^{98}(FG2)	NH	8.72	7.27
	$C_\beta H$	3.61	1.36	Val^{101}(FG5)	$C_\beta H$	1.21	2.73
Lys^{67}(E10)	$C_\gamma H$	0.27	1.58		$C_\gamma H_3$	−0.48	1.26
	$C_\delta H$	0.01	0.22		$C_{\gamma'} H_3$	0.15	0.66
	$C_\varepsilon H$	1.49	3.32	Phe^{106}(G5)	$C_\varepsilon H$	7.12	6.87
Phe^{68}(E11)	NH	9.17	8.61		$C_\zeta H$	7.92	7.05
	$C_\alpha H$	1.81	5.22	Val^{109}(G8)	$C_\alpha H$	2.13	3.45
	$C_\beta H$	5.56	3.23		$C_\beta H$	0.11	2.83
	$C_{\beta'} H$	2.64	2.92		$C_\gamma H_3$	−0.06	1.16
	$C_\delta H$	6.39	5.77		$C_{\gamma'} H_3$	−1.14	0.94
	$C_\varepsilon H$	6.78	5.75	Val^{140}(H15)	$C_\alpha H$	1.9	3.57
Val^{71}(E14)	$C_\alpha H$	2.71	3.94		$C_\beta H$	1.44	2.06
	$C_\beta H$	1.02	3.02		$C_\gamma H_3$	0.51	1.16
	$C_\gamma H_3$	0.2	2.20	Trp^{148}(H23)	$C_{\varepsilon 3H}$	8.08	6.38
	$C_{\gamma'} H_3$	−1.27	2.08		$C_{h2}H$	8.49	6.78
Leu^{92}(F4)	NH	8.76	7.40				

Observed chemical shifts δ_{DSS}(obs) in ppm are referenced to DSS in ^1H_2O 100 mM phosphate, pH 7.5 at 300 K. Diamagnetic chemical shifts, δ_{DSS}(dia), calculated via Eq. (4) using the NgbCO crystal coordinates.

2.2. NMR spectroscopy

^{1}H NMR data were collected on a Brucker AVANCE 600 spectrometer operating at 600 MHz for protein samples in both ^1H_2O and ^2H_2O over the temperature range 5–30 °C. Unless otherwise stated, all spectra were recorded with a repetition rate of 1 s^{-1} and chemical shifts were indirectly referenced to 2,2-dimethyl-2-silapentane-5-sulfonate (DSS) through the water resonance calibrated at each temperature. 1D reference spectra were recorded with the standard 90° pulse sequence with presaturation of the water solvent signal, and WEFT [37] spectra were recorded to detect broad, fast relaxed proton signals (Fig. 2).

Non-selective T_1s were determined to ±15% uncertainty at 30 °C for resolved and fast relaxed protons from the initial magnetization recovery of a standard inversion- recovery pulse sequence. The distance

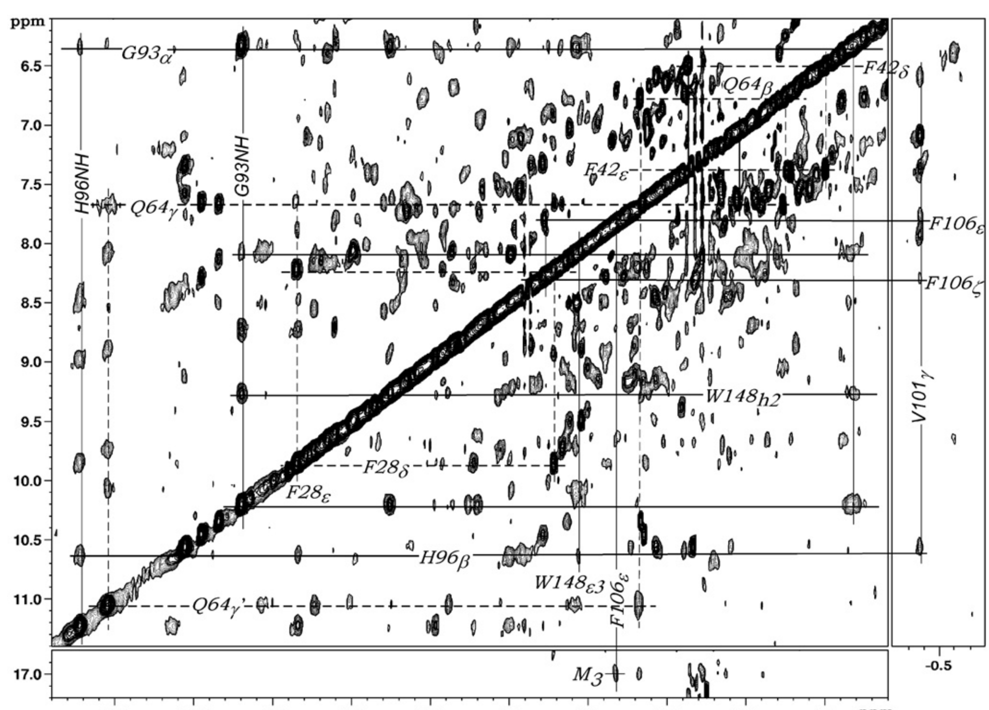

Fig. 4. Portions of the NOESY spectrum of dm-metNgbCN in ^1H_2O at 300 K that illustrates the dipolar contacts between heme and active site residues for isomer B. The solid lines represent proximal dipolar contacts and the dashed lines represent distal dipolar contacts.

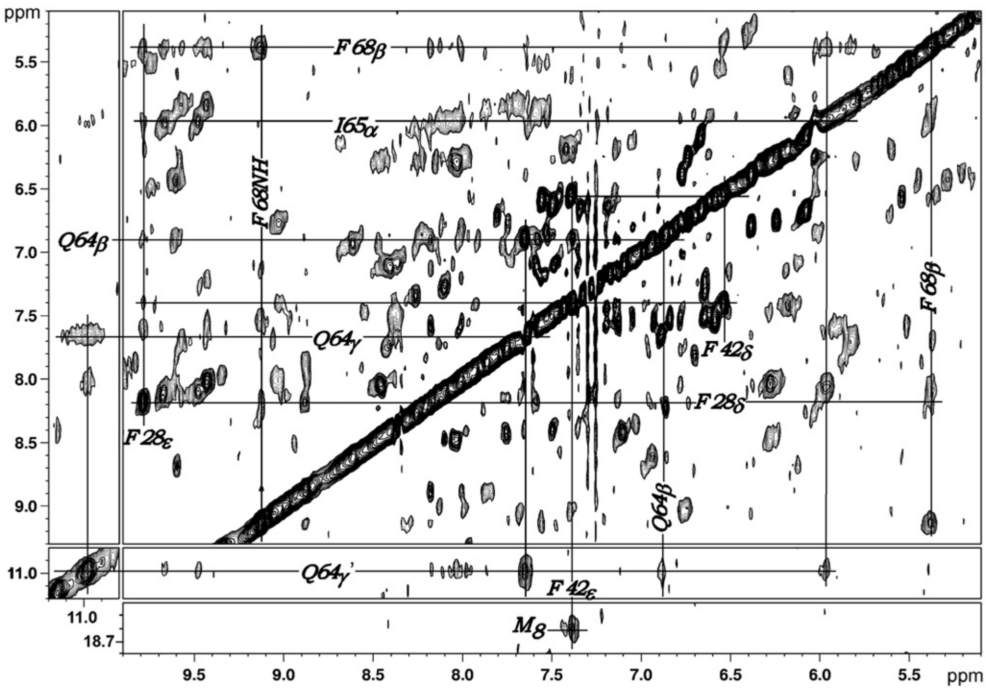

Fig. 5. Portions of the NOESY spectrum of dm-metNgbCN in ^2H_2O at 303 K that illustrates the dipolar contacts between C_εHs of Phe[28](B10) and C_βH of Gln[64](E7), C_αH of Ile[65](E8), C_βH of Phe[68](E11), C_εHs of Phe[42](CD1); between C_εHs of Phe[42](CD1) and C_βH of Gln[64](E7), between C_αH of Ile[65](E8) and C_γH of Gln[64](E7), which uniquely characterize the orientation of the E7 side chain.

$R_{\mathrm{Fe-H}i}$ of proton H_i with T_{1i} from the iron centre was estimated using Eq. (1), which is defined as,

$$R_{\mathrm{Fe-}Hi} = R^*_{\mathrm{Fe-}H}\left(\frac{T_{1i}}{T_1^*}\right)^{\frac{1}{6}} \quad (1)$$

where $R^*_{\mathrm{Fe-H}}$ and $T_1{}^*$ are the reference distance and its associated T_1 value. $R_{\mathrm{Fe-H}i}$ distances were estimated by using two set of reference values [27], the heme 8-CH_3 for which $R^*_{\mathrm{Fe-H}}$=6.10 Å and $T_1{}^*$=126 ms, and F8 N_δH for which $R^*_{\mathrm{Fe-H}}$=5.07 Å and $T_1{}^*$=34 ms as the upper and lower limits for a proton of interest.

NOESY [38] and TOCSY [39] data were collected ($512t_1\times2048t_2$) in order to identify dipolar and scalar connectivities. Spectral widths of 13 kHz and mixing time of 75 ms for NOESY and 40 ms for TOCSY were used. The 90° pulse width was about 9 μs (about 20 μs for TOCSY spin lock). 192 scans were collected for each block. Two dimensional data sets were processed by Bruker Xwinnmr or Topspin software. Both NOESY and TOCSY spectra were processed by a 30°-shifted-sine-squared-bell apodization and zero-filled to 2048×2048 complex points prior to Fourier transformation.

2.3. Magnetic axes determination

With chemical shift temperature gradients [40], the experimental dipolar shifts of backbone protons and the protons of the structurally conserved residues were used in a non-linear least squares regression fit of Eq. (2) to determine the Euler rotation angles α, β, γ of the magnetic tensor. The Euler angles, transform the molecular pseudosymmetry coordinate axes x', y' and z' (Fig. 3) identified from crystal coordinates (PDB code 1W92) [25] into the magnetic axes x, y, and z, by minimizing the error function F according to the following equation [41]:

$$F/n = \sum\left[\left|\delta_{\mathrm{dip}}(\mathrm{obs}) - \delta_{\mathrm{dip}}(\mathrm{calc})\Gamma(\alpha,\beta,\gamma)\right|\right]^2 \quad (2)$$

where

$$\delta_{\mathrm{dip}}(\mathrm{calc}) = (12\pi\mu N_0)^{-1}\left[2\Delta\chi_{ax}(3\cos^2\theta' - 1)R^{-3} + 3\left(\Delta\chi_{rh}\sin^2\theta'\cos2\Omega'\right)R^{-3}\right] \quad (3)$$

$$\delta_{\mathrm{dip}}(\mathrm{obs}) = \delta_{\mathrm{DSS}}(\mathrm{obs}) - \delta_{\mathrm{DSS}}(\mathrm{dia}) \quad (4)$$

n is the number of δ_{dip}(obs), δ_{DSS}(obs) and δ_{DSS}(dia) are the chemical shifts, in ppm, referenced to DSS, for the paramagnetic mouse dm-metNgbCN complex and an isostructural diamagnetic complex respectively. Despite the absence of experimentally determined δ_{DSS} (dia), they can be reasonably estimated from the available crystal structure using

$$\delta_{\mathrm{DSS}}(\mathrm{dia}) = \delta_{\mathrm{tetr}} + \delta_{\mathrm{sec}} + \delta_{\mathrm{rc}} \quad (5)$$

where δ_{tetr}, and δ_{sec} are the chemical shifts from an unfolded tetrapeptide [42] and the effect of secondary structure [43]. And δ_{rc} is the chemical shift of the ring current [44] from the heme and the ring protons of aromatic residues as described in detail previously [45].

2.4. Structural modeling

Protons were added to the crystal coordinates of NgbCO using Sybyl software (Tripos) [46] on a Linux platform. The coordinates of mutant Gln[64] and Phe[68] were introduced into the PDB file using the Biopolymer program in Tripos software package. The CN^- position was determined from magnetic axes parameter and added into the coordinates file. The buildup model was carried out an energy minimization protocol. A total 3000 cycles under Amber ff94 force field was used for the whole system to remove the unfavorable steric contacts. The obtained simulation structure was further utilized to locate the solution structure of side chains for residue Gln[64](E7), Phe[68](E11) and Phe[28](B10) predominantly, associated with the observed dipolar shifts and the magnetic axes parameters [47].

3. Results

The ^{1}H NMR spectra of mouse dm-Ngb cyanomet complex is illustrated in Fig. 2A. Based on NMR signal intensities, it is interesting to observe two isomers (labeled A and B) that equilibrates to about 1:1 upon ligation of cyanide. Isomer A has the same heme orientation as that found in SWMb which is characterized by the NOE dipolar contacts of the heme 5-CH_3 to the side chain of CD1 [48,49]. On the other hand, for isomer B the heme orientation is rotated by 180° with

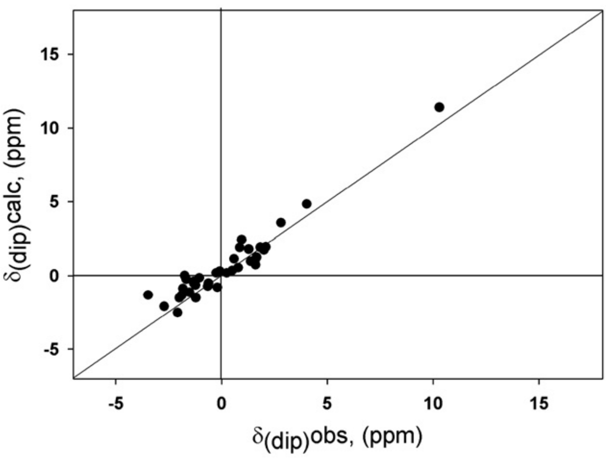

Fig. 6. Correlation between observed and calculated dipolar shifts for mouse dm-metNgbCN for the optimized magnetic axes α=0°, β=8°, κ=α+γ=15° with the $\Delta\chi_{ax}$=1.8×10^{-8} m^3/mol, $\Delta\chi_{rh}$=−0.20×10^{-8} m^3/mol obtained from isomer B of dm-metNgbCN.

respect to the α–γ meso axis, and it is characterized by the NOE dipolar contacts of the heme 8-CH_3 to the side chain of CD1 (Fig. 3). The protons of the heme and His^{96}(F8) residues of isomers A and B could be readily assigned, while most other residues far away from iron center could not be easily distinguished due to spectral overlap. Herein we report and characterize the atypical B isomer of the mouse dm-metNgbCN complex.

3.1. Resonance assignments

Representative 1D ^{1}H NMR spectra of mouse dm-metNgbCN in ^1H_2O and ^2H_2O are illustrated in Fig. 2A and B. A WEFT spectrum designed to emphasize fast relaxed proton signals (e.g. C_ζH of Phe^{28}) is shown in Fig. 2C. Assignments deduced herein are given by the Fischer heme notation and the standard amino acid one-letter code. Due to (sometimes severe) signal overlap, of the two isomers, assignment of heme pocket residues were pursued to the fullest extent possible using backbone connectivities as a standard method for diamagnetic proteins [50]. Target residues which could not be identified by these standard methods were assigned from residue-heme and inter-residue NOESY cross-peaks, relaxation parameters and/or partial TOCSY cross-peaks. The identification of hyperfine shifted and relaxed resonances were greatly facilitated by variable temperature studies which help to identify scalar/dipolar connectivities [51]. The chemical shifts for heme and His^{96}(F8) are listed in Table 1, and those for key residues are listed in Table 2. Non-selective T_1 values for predominantly paramagnetically influenced protons are given in parentheses.

3.2. Heme assignments

The heme substituents were unambiguously assigned using methods described in detail elsewhere [52]. Briefly, two TOCSY-detected vinyl and propionate groups exhibit significant hyperfine shifts and NOESY cross-peaks to low field resolved methyls that uniquely assign the 3-CH_3 and 4-vinyl, and 8-CH_3 and 7-propionate. Strong hyperfine shifts and NOESY cross-peaks between 6-propionate, 4-β and the heme methyl assign the 5-CH_3. NOESY cross-peaks between 8-CH_3 and an unidentified, 3-proton integrated peak assign the unidentified peak as the 1-CH_3. Some of heme assignments for isomer A were identified and listed in Table 1 as well.

3.3. Assignments of key resolved resonances

The resonance at 15.84 ppm (T_1≈34 ms) from a D_2O exchangeable (i.e. labile) proton can be assigned as N_δH of His^{96}(F8) as it exhibits NOE cross-peaks to a resonance from a labile proton at 11.22 ppm, which is TOCSY/NOESY connected to a spin system diagnostic of the axial His^{96}(F8) $C_\beta H_2$-C_αH-NH fragment. TOCSY-detected C_αH-NH backbone and C_βHs of residues of the F-helix, i.e. Lys^{92}(F4) through Thr^{98}(FG2), could be identified through the typical N_i–N_{i+1}, α_i–N_{i+1}, β_i–N_{i+1} contacts observed for helices. In addition, the expected cross peak between the Gly^{93}(F5) C_αH proton and His^{96}(F8) NH identifies the F-helix assignments (see supporting information for sequential connectivities).

TOCSY connections, involving a set of upfield hyperfine shifted resonances, are attributed to an AM(X_3)(Y_3) spin system. The dipolar contacts to 8-CH_3 and 1-CH_3 uniquely identify this residue as Val^{101}(FG5). Aromatic ring protons with NOESY cross-peaks to 3-CH_3 and the Val^{101}(FG5) side chain, are identified as the C_δHs of Phe^{106}(G5). Additional key assignments, including NOESY cross-peaks between the C_αHs of Gly^{93}(F5) and C_ζHs of Trp^{148}(H23); C_γHs of Val^{140}(H15) and C_βHs of 4-vinyl and 3-CH_3; C_γHs of Val^{109}(G8) and 3-CH_3 were used to assist with the determination of the heme ring orientation. Fig. 4 gives the key dipolar contacts between heme and active site residues.

A set of TOCSY-connected protons in the downfield region dictates its arise from the distal residue Phe^{28}(B10) (see supporting materials), the resolved (14.73 ppm), fast relaxed (T_1=49 ms), non-labile single proton peak is from C_ζH of Phe^{28}(B10), which is similar to that found in WT-metNgbCN [22]. TOCSY-connected protons which exhibit NOESY cross-peaks with 4-vinyl and 5-CH_3 are assigned to Val^{71}(E14). The Phe^{42}(CD1) ring exhibits NOESY cross-peaks to C_εHs of Phe^{28}(B10) and 8-CH_3 of the heme, but not to 5-CH_3 in isomer B, which clearly confirm that the heme is rotated by 180° about the α, γ-meso axis as observed in the crystal structure [23]. The rotation of the heme ring is further confirmed by the characteristic dipolar contacts between Val^{101}(FG5) and 8-CH_3, and Val^{71}(E14) and 5-CH_3. Observed NOESY cross-peaks between a set of aromatic ring protons and the C_δHs from Phe^{42}(CD1) and Phe^{28}(B10) identify the ring is from Phe^{32}(B14). NOESY cross-peaks observed between 5-CH_3, C_βHs of 6-propionate and two upfield protons, which belong to a long side chain spin system, identify the distal residue Lys^{67}(E10). Other key NOESY connections include cross-peaks between C_εHs of Phe^{28}(B10) and C_βHs of Gln^{64}(E7), C_αH of Ile^{65}(E8), C_βHs of Phe^{68}(E11) (Fig. 5). The E-helix was identified by observed NOESY contacts between C_αH of Ile^{65}(E8) and C_βH of Phe^{68}(E11), C_δHs of Lys^{67}(E10) and NH of Phe^{68}(E11), and C_βH of Gln^{64}(E7) and 7-propionate.

A non-labile, very broad and strongly relaxed resonance with linewidth ≈500 Hz (T_1≈5 ms) and integrated intensity corresponding

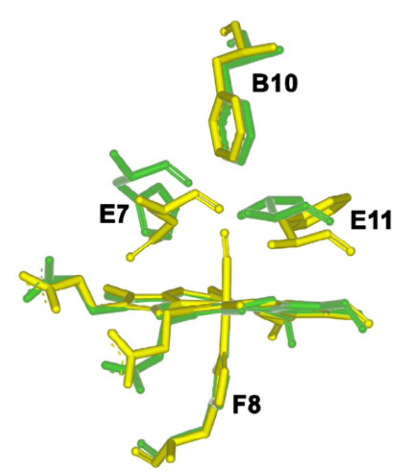

Fig. 7. Comparison of the distal pocket structure of dm-metNgbCN and NgbCO. The $N_\varepsilon H_1$ atom of Gln^{64}(E7) is in a position that may form hydrogen bond with the ligated cyanide and occupies a position similar to that of a corresponding atom in His64 which is found in almost all mammalian myoglobins. Green represents mouse NgbCO and yellow represents the modified distal structure of dm-NgbCN in solution.

to a single proton is observed at −7.12 ppm. Such broad signal possibly arises from the non-labile ring $C_{\varepsilon}H$ proton of His[96](F8), according to deduction of chemical shift occurred especially in this upfield region, as in some cases of Mb. However, the resonance remains unassigned.

3.4. Magnetic axes

Using the available set of NgbCO crystal coordinates(PDB code: 1W92), and the δ_{dip}(obs) values calculated from Eq. (4) for all assigned residues (except B10, E7 and E11) with significant temperature dependence of their chemical shifts, the five parameters $\Delta\chi_{ax}$, $\Delta\chi_{rh}$, α, β and κ (where $\kappa=\alpha+\gamma$) were determined from a non-linear least squares regression search of Eq. (2). To confirm proton assignments and the distance from the iron centre, multiple least squares regression searches were performed by varying the number of input δ_{dip}(obs) values, in order to obtain undoubted magnetic parameters. Based on the search with all 30 δ_{dip}(obs) values, the magnetic axis parameters were determined to be: $\alpha=0\pm10°$, $\beta=8.0\pm5.0°$ and $\kappa=\alpha+\gamma=15\pm5°$ and yielded $\Delta\chi_{ax}=1.8\pm0.3\times10^{-8}$ m^3/mol and $\Delta\chi_{rh}=-0.2\pm0.3\times10^{-8}$ m^3/mol, which are within the uncertainties of the inputted data sets. The residual error function $F/n=0.10$ ppm^2 represents a good correlation between observed and calculated dipolar shifts (Fig. 6). There are no obvious outliers in Fig. 6 and the good linearity reflects the justification for using crystal structure to calculate the diamagnetic shifts and the similarity between the WT and double mutant. Therefore, based on the calculated dipolar shift, the relaxation property ($T_1=22$ ms), and a distance from the iron center (4.6± 0.2), a downfield hyperfine shifted resonances at 11.77 ppm, is uniquely assigned to the $N_{\varepsilon}H_1$ of Gln[64](E7) since it is the only labile proton close to the iron atom at such a distance in heme pocket. Considering the uncertainty of the distance restraints and taking protons of F8 $N_{\delta}H$ and heme 8-methyl as references, the T_1 based distance restraints R_{Fe-Hi}, calculated by Eq. (1), have been listed in Table 1S with corresponding T_1 values (see supporting materials), and all of these data can match the experimental data and be used for conformational analysis.

The tilt of the major magnetic axes is correlated with Fe–CN tilt which is observed in WT-metMbCN complexes [35,45,53]. The rhombic axis defined by $\kappa=15°$, has a slight difference from the ϕ angle identified from the crystal structure of NgbCO (Fig. 3). A Curie plot of observed shift versus inverse of absolute temperature for most peaks including Phe[28](B10) side chain ring protons (see supporting materials for representative peaks) exhibits good linear correlation. It represents reasonable assignments for the peaks which are consistent with the sign of dipolar shifts.

3.5. Structural simulation

The simulated structure shows a RMSD of 2.8 Å for all backbone atoms compared with crystal structure of NgbCO. Then using methods described in detail by Qin et al. [47], the orientation of Gln[64](E7) in dm-metNgbCN was refined after simulation by searching for the side chain rotation angles, χ_1, χ_2 and χ_3 which represent the best static fit and reproduce the magnetic axes and the δ_{dip}(obs) shifts well. The magnetic axes and δ_{dip}(obs) shifts could be better described by an orientation of Gln[64](E7) corresponding to $\chi_1=61°$, $\chi_2=135°$, $\chi_3=140°$. And the distance between iron atom and $N_{\varepsilon}H_1$ of E7 is 4.6±0.2 Å, a distance which is consistent with that obtained independently by relaxation data.

The backbone protons of E11 are confirmed by the dipolar contacts of Phe[68](E11) C_{β}Hs to CεHs of Phe[28](B10). The side chain of Phe[68](E11) is solidly assigned with observable dipolar contacts of the C_{δ}Hs, C_{ε}Hs and C_{β}H of Phe[68](E11) to the 4-vinyl. From these dipolar contacts, the orientation of Phe[68](E11) places the side chain rotation angles at $\chi_1=59°$ and $\chi_2=120°$, which lead to good correlations between observed and calculated dipolar shifts for E11 protons.

Observed dipolar shifts for the Phe[28](B10) C_{ζ}H and C_{ε}Hs, based on the modified dm-metNgbCN coordinates, are not included in magnetic axes determination. Interestingly, the observed dipolar shifts of Phe[28](B10) is very close to the calculated dipolar shifts. Further, the calculated and observed dipolar shifts for the C_{δ}Hs and C_{ε}Hs of another aromatic residue on the distal side, Phe[42](CD1), are well predicted. In addition, the dipolar shift of Phe[28](B10) C_{ζ}H indicates a reasonable distance of Phe[28](B10) C_{ζ}H to heme iron atom with $R_{Fe}(C_{\zeta}H)=5.3\pm0.1$ Å. The orientation of Phe[28](B10) (Fig. 7) in dm-metNgbCN is thus, identified to be very similar to that found in the NgbCO crystal structure.

4. Discussion

4.1. Structural heterogeneity of dm-metNgbCN

Two sets of NMR resonances for heme protons and protons within the active site are indicative and typical of two different heme orientation isomers A and B (Fig. 2). From the integrated intensity, the population ratio is about 1:1 for isomer A:B, which is consistent with observations

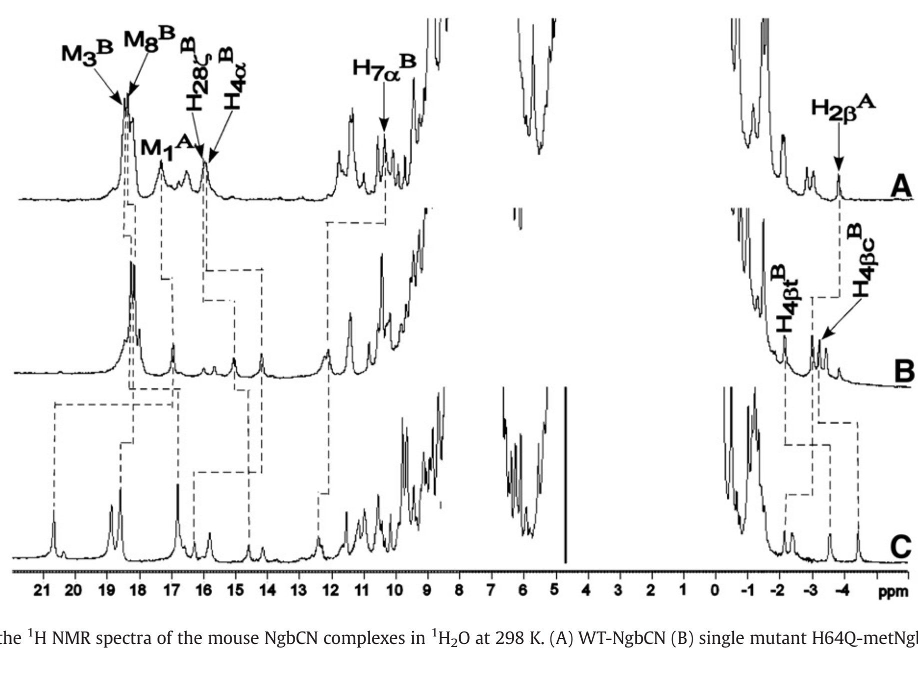

Fig. 8. Comparison of the ^{1}H NMR spectra of the mouse NgbCN complexes in ^1H_2O at 298 K. (A) WT-NgbCN (B) single mutant H64Q-metNgbCN (C) dm-metNgbCN.

reported by La Mar et al. for WT-metNgbCN [22]. They determined that the heme orientational disorder changes from about 1:2 (for A:B) in mouse WT-metNgb to about 1:1 upon binding of cyanide. Since for the H64Q/V68F double mutant Ngb, His^{64} was replaced by Gln^{64}, the rupture of the E7 bond to the iron was not observed, and the ligand bound complex formed rapidly after addition of CN^-. By comparing 1D ^1H NMR spectra between WT-metNgbCN (Fig. 8A), single mutant H64Q-metNgbCN (Fig. 8B, Du and La Mar et al., unpublished) and dm-metNgbCN (Fig. 8C), the heme methyl protons (3-CH_3 and 8-CH_3 for isomer B, and 1-CH_3 and 5-CH_3 for isomer A) are all located in downfield regions and have a set of similar relaxation rates. All of the three cyanide complexes display a similar population ratio of 1:1 for isomer A to B. From the X-ray structure of mouse metNgb, two heme conformations with a population ratio of 30:70 (for A:B, and A is the same as in SWMb) [23] are observed. Therefore, it is possible that external ligand binding induces a mean heme re-equilibration to 1:1. The population of two NgbCN isomers in solution seems not to be affected by the mutation of single or double mutants at E7 and E11 position.

4.2. Magnetic properties

The mouse double mutant H64Q/V68F NgbCN is the first example to obtain unique magnetic axes parameters for neuroglobin family. The determination of the magnetic axes based on crystal coordinates of NgbCO yields five parameters. These parameters reflect variable heme orientation that impacts proton dipolar shifts. The axial anisotropy $\Delta\chi_{ax} \approx 1.8 \times 10^{-8}$ m^3/mol and the rhombic anisotropy $\Delta\chi_{rh} \approx -0.2 \times 10^{-8}$ m^3/mol are both significantly smaller than those found in metMbCN and metHbCN complexes [54,55]. The tilt $\beta \approx 8°$ and the direction of the tilt $\alpha \approx 0°$ of the major magnetic axis possibly lead to the nitrogen atom of cyanide acting as a H-bond acceptor to E7 $N_\varepsilon H_1$. The value of $k \approx 15°$ is consistent with an effective rhombic perturbation and provides additional confirmation of the comparable orientation of His^{96}(F8) imidazole plane with $\phi \approx 22°$ by the analysis of Walker [56] and in the crystal structure of NgbCO, as illustrated in Fig. 3. For the dm-metNgb mutant, the heme orientation of isomer B is, in fact, rotated 180° along with the α–γ-meso axis, different from that in mammalian globins (CD1 near the 5- CH_3 of heme)(Figs. 3 and 5), but is consistent with the unique isomer of NgbCO crystal structure. Moreover, both the good correlation of observed and calculated dipolar shifts (Fig. 6), and the similarity of the ligated spectra of the WT and double mutant(Fig. 8) reflect the justification for using crystal coordinates to obtain the reliable magnetic axes.

4.3. Active site structure

The ^1H NMR data for the proximal side of the heme group in cyanide complex of mouse dm-Ngb indicate a highly conserved molecular structure as found in mouse WT-Ngb. Local structural changes are observed in the vicinity of the distal mutation. However, the introduction of point mutation in the distal pocket yields a comparatively unperturbed proximal side. The dipolar contacts between residues and heme, or between distal residues in dm-metNgbCN are essentially the same as those observed for mouse WT-metNgbCN (Fig. 3). Slight differences in dipolar shifts are observed, for instance the Val101(FG5), and are possibly due to the difference in magnetic axes.

In the solution NMR study on murine Ngb [22], the binding process of CN^- with WT-Ngb experienced nearly hours to complete the binding to heme iron. At present work, after double mutations of this protein, the total CN^- binding process spent only several minutes within NMR acquisition time limit. Such a variation of dynamic feature in binding rates suggests the two mutated sites having a notable influence on modulation of ligand affinities. And the distal side structure has been rearranged due to mutations (Fig. 7).

Gln64(E7) in dm-metNgbCN occupies a position different from that of His64(E7) in WT-NgbCO crystal structure. The orientation of the side chain is in a position to possibly form a hydrogen bond with the cyanide ligand and the distance of E7 $N_\varepsilon H_1$ to the heme iron is about 4.6 Å, therefore $N_\varepsilon H_1$ acts as a H-bond donor in this case (Fig. 7), just like its role in triple mutants of SWMbCN. Based on the analysis of the assigned resonances and observed dipolar shifts for Phe^{68}(E11), the position and orientation of this residue are similar to that observed in triple mutants of SWMbCN [27]. This is not surprising as the point mutation at E11 plays an important role on properties of heme cavity which is crowded by neighboring aromatic residues (CD1 and B10) on the distal side. The position of the B10 aromatic ring of the dm-Ngb appears to be similar to that of NgbCO, which is in van der Waals contact with the bound ligand. The Phe^{28}(B10) side chain is closer to the heme iron with the distance of $C_\zeta H$ to iron being 5.30 Å.

As a result, Gln^{64} may participate to form hydrogen bond that stabilizes the ligand [27,28,32,33]. Although to some extent heme methyls display different contact shifts (see Fig. 8), it is possible that the substitution of Gln side chain for the bulky imidazole side chain of E7 in the H64Q/V68F mutant contributes to the difference in ligand tilt from that in WT. Similar to the example in Mb [28], E11 has van der Waals steric contact with the ligand. The presence of aromatic ring in E11, could stabilize the conformation via a π–π stacking interaction with B10, CD1 and the heme. Hence, the E7 and E11 residues appear to control the direction and the extent of tilt of the bound ligand, respectively. The tilt of ligand has no obvious influence on the heme heterogeneity of cyanide complex of the WT and mutant protein, implicating that the factors other than steric effects, such as polarity of heme pocket, play an important role in modulating ligand binding.

4.4. Comparison of neuroglobin with cytoglobin in solution structure

The mouse WT-metNgb yields a 2:1 ratio of isomer B to A in solution [22], moreover, both the WT-Ngb and the double mutant H64Q/V68F-Ngb show structural heterogeneities with population ratio of about 1:1 when cyanide is ligated (Fig. 2). Whereas the structural heterogeneities of another bis-histidyl coordinated vertebrate globin, Cgb are not so prevalent in its ferric form in solution [57]. The heme orientation of Cgb adopts a major A conformation similar to that in SWMb and the population ratio of A to B is about 90:10. It is indicative of Ngb having a larger heme pocket than Cgb. Although no external CN^- ligated Cgb structure is reported at present, the structural difference seems to correlate with the ligand binding affinity and heme cavity properties [58,59]. These two new members of the globin family, Ngb and Cgb, will be examined in greater detail as we are interested in the physiological function of them, such as O_2 sensing, enzymatic activity and/or signal transduction.

Acknowledgements

We thank Prof. Gerd N. La Mar (Department of Chemistry, University of California at Davis, USA) for the friendly discussion and supports. This work was supported by the National Natural Science Foundation of China (20473013) and by the National Basic Research Program of China (2004CB719900) as well as the Key Project of Chinese Ministry of Education No.105010.

Appendix A. Supplementary data

Supplementary data associated with this article can be found, in the online version, at doi:10.1016/j.bpc.2008.05.003.

References

[1] T. Burmester, B. Weich, S. Reinhardt, T. Hankeln, A vertebrate globin expressed in the brain, Nature 407 (2000) 520–523.
[2] M. Brunori, B. Vallone, Neuroglobin, seven years later, Cell. Mol. Life Sci. 64 (2007) 1259–1268.
[3] T. Burmester, T. Hankeln, Neuroglobin: A respiratory protein of the nervous system, News Physiol. Sci. 19(2004) 110–113.

[4] A. Pesce, M. Bolognesi, A. Bocedi, P. Ascenzi, S. Dewilde, L. Moens, T. Hankeln, T. Burmester, Neuroglobin and cytoglobin, fresh blood for the vertebrate globin family, EMBO Rep. 3 (2002) 1146–1151.

[5] Y. Sun, K. Jin, X.O. Mao, D.A. Zhu, Neuroglobin is upregulated by and protects neurons from hypoxic-ischemic injury, Proc. Natl. Acad. Sci. U. S. A. 98 (2001) 15306–15311.

[6] K. Wakasugi, T. Nakano, C. Kitatsuji, I. Morishima, Human neuroglobin interacts with flotillin-1, a lipid raft microdomain-associated protein, Biochem. Biophys. Res. Commun. 318 (2004) 453–460.

[7] A.A. Khan, X.O. Mao, S. Banwait, K. Jin, D.A. Greenberg, Neuroglobin attenuates β-amyloid neurotoxicity in vitro and transgenic Alzheimer phenotype in vivo, Proc. Natl. Acad. Sci. U. S. A. 104 (2008) 19114–19119.

[8] M. Couture, T. Burmester, T. Hankeln, D.L. Rousseau, The heme environment of mouse neuroglobin, J. Biol. Chem. 276 (2001) 36377–36382.

[9] J.T.I. Trent, R.A. Watts, M.S. Hargrove, Human neuroglobin, a hexacoordinate hemoglobin that reversibly binds oxygen, J. Biol. Chem. 276 (2001) 30106–30110.

[10] S. Dewilde, L. Kiger, T. Burmester, T. Hankeln, V. Baudin-Creuza, T. Aerts, M.C. Marden, R. Caubergs, L. Moens, Biochemical characterization and ligand binding properties of neuroglobin, a novel member of the globin family, J. Biol. Chem. 276 (2001) 38949–38955.

[11] V.S. Nistor, E. Goovaerts, S. van Doorslaer, S. Dewilde, L. Moens, NO binding properties of neuroglobin, A characterization by EPR and flash photolysis, Chem. Phys. Lett. 361 (2002) 355–361.

[12] S. van Doorslaer, S. Dewilde, L. Kiger, S.V. Nistor, E. Goovaerts, M.C. Marden, L. Moens, Nitric oxide binding properties of neuroglobin, J. Biol. Chem. 278 (2003) 4919–4925.

[13] M. Couture, T.K. Das, H.C. Lee, J. Peisach, D.L. Rousseau, B.A. Wittenberg, J.B. Wittenberg, M. Guertin, *Chlamydomonas chloroplast* ferrous hemoglobin, heme pocket structure and reactions with ligands, J. Biol. Chem. 274 (1999) 6898–6910.

[14] M. Couture, T.K. Das, P.Y. Savard, Y. Ouellet, J.B. Wittenberg, B.A. Wittenberg, D.L. Rousseau, M. Guertin, Structural investigations of the hemoglobin of the cyanobacterium *Synechocystis* PCC6803 reveal a unique distal heme pocket, Eur. J. Biochem. 267 (2000) 4770–4780.

[15] N.L. Scott, C.J. Falzone, D.A. Vuletich, J. Zhao, D.A. Bryant, J.T. Lecomte, Truncated hemoglobin from the cyanobacterium *Synechococcus* sp. PCC 7002: evidence for hexacoordination and covalent adduct formation in the ferric recombinant protein, Biochemistry 41 (2002) 6902–6910.

[16] T. Burmester, B. Ebner, B. Weich, T. Hankeln, Cytoglobin: a novel globin type ubiquitously expressed in vertebrate tissues, Mol. Biol. Evol. 19 (2002) 416–421.

[17] E. Vinck, S. van Doorslaer, S. Dewilde, L. Moens, Structural change of the heme pocket due to disulfide bridge formation is significantly larger for neuroglobin than for cytoglobin, J. Am. Chem. Soc. 126 (2004) 4516–4517.

[18] T.R. Weiland, S. Kundu, J.T. Trent, J.A. Hoy, M.S. Hargrove, Bis-histidyl hexacoordination in hemoglobins facilitates heme reduction kinetics, J. Am. Chem. Soc. 126 (2004) 11930–11935.

[19] T. Hankeln, B. Ebner, C. Fuchs, F. Gerlach, M. Haberkamp, T.L. Laufs, A. Roesner, M. Schmidt, B. Weich, S. Wystub, S. Saaler-Reinhardt, S. Reuss, M. Bolognesi, D. de Sanctis, M.C. Marden, L. Kiger, L. Moens, S. Dewilde, E. Nevo, A. Avivi, R.E. Weber, A. Fago, T. Burmester, Neuroglobin and cytoglobin in search of their role in the vertebrate globin family, J. Inorg. Biochem. 99 (2005) 110–119.

[20] K. Shikama, A. Matsuoka, Structure–function relationships in unusual nonvertebrate globins, Crit. Rev. Biochem. Mol. Biol. 39 (2004) 217–259.

[21] K. Nienhaus, J.M. Kriegl, G.U. Nienhaus, Structural dynamics in the active site of murine neuroglobin and its effects on ligand binding, J. Biol. Chem. 279 (2004) 22944–22952.

[22] W.H. Du, R. Syvitski, S. Dewilde, L. Moens, G.N. La Mar, Solution ^{1}H NMR characterization of equilibrium heme orientational disorder with functional consequences in mouse neuroglobin, J. Am. Chem. Soc. 125 (2003) 8080–8081.

[23] A. Pesce, S. Dewilde, M. Nardini, L. Moens, P. Ascenzi, T. Hankeln, T. Burmester, M. Bolognesi, Human brain neuroglobin structure reveals a distinct mode of controlling oxygen affinity, Structure 11 (2003) 1087–1095.

[24] B. Vallone, K. Nienhaus, M. Brunori, G.U. Nienhaus, The structure of murine neuroglobin: Novel pathways for ligand migration and binding, Proteins 56 (2004) 85–92.

[25] B. Vallone, K. Nienhaus, A. Matthes, M. Brunori, G.U. Nienhaus, The structure of carbonmonoxy neuroglobin reveals a heme-sliding mechanism for control of ligand affinity, Proc. Natl. Acad. Sci. U. S. A. 101 (2004) 17351–17356.

[26] R.F. Tilton Jr., I.D. Kuntz Jr., G.A. Petsko, Cavities in proteins: structure of a metmyoglobin xenon complex solved to 1.9 ANG, Biochemistry 23 (1984) 2849–2857.

[27] B.D. Nguyen, X.F. Zhao, K. Vyas, G.N. La Mar, R.A. Lile, E.A. Bruker, G.N. Philips Jr., J.S. Olson, J.B. Wittenberg, Solution and crystal structures of a sperm whale myoglobin triple mutant that mimics the sulfide-binding hemoglobin from *Lucina pectinata*, J. Biol. Chem. 273 (1998) 9517–9526.

[28] K. Rajarathnam, J. Qin, G.N. La Mar, M.L. Chiu, S.G. Sligar, Correlation between the steric bulk of the distal E7 and E11 residues and the tilt of the FeCN unit in cyanometmyoglobin as determined by NMR from the orientation of the magnetic axes in single and double point mutants, Biochemistry 33 (1994) 5493–5501.

[29] A. Fago, A.J. Mathews, L. Moens, S. Dewilde, T. Brittain, The reaction of neuroglobin with potential redox protein partners cytochrome b_5 and cytochrome c, FEBS Lett. 580 (2006) 4884–4888.

[30] T. Uno, D. Ryu, H. Tsutsumi, Y. Tomisugi, Y. Ishikawa, A.J. Wilkson, H. Sato, T. Hayashi, Residues in the distal heme pocket of neuroglobin: implications for the multiple ligand binding steps, J. Biol. Chem. 279 (2004) 5886–5893.

[31] J. Qin, U. Pande, G.N. La Mar, F. Ascoli, P. Ascenzi, F. Cutruzzola, C. Travaglini-Allocatelli, M. Brunori, ^{1}H NMR study of the dynamics of the pH modulation of axial coordination in *Aplysia Limacina* (Val(E7)) and *sperm whale* double mutant His(E7)- Val,Thr(ElO)-Arg metmyoglobin, J. Biol. Chem. 268 (1993) 24012–24021.

[32] G.N. La Mar, F. Dalichow, X.F. Zhao, Y. Dou, M. Ikeda-Saito, M.L. Chiu, S.G. Sliga, ^{1}H NMR investigation of distal mutant deoxy myoglobins, J. Biol. Chem. 269 (1994) 29629–29635.

[33] B.A. Springer, K.D. Egeberg, S.G. Sligar, R.J. Rohlfs, A.J. Mathews, J.S. Olson, Discrimination between oxygen and carbon monoxide and inhibition of autooxidation by myoglobin. Site-directed mutagenesis of the distal histidine, J. Biol. Chem. 264 (1989) 3057–3060.

[34] M. Rizzi, J.B. Wittenberg, A. Coda, M. Fasano, P. Ascenzi, M. Bolognesi, Structure of the sulfide-reactive hemoglobin from the clam *Lucina pectinata*. Crystallographic analysis at 1.5 A resolution, J. Mol. Biol. 244 (1994) 86–99.

[35] X.F. Zhao, K. Vyas, B.D. Nquyen, K. Rajarathnam, G.N. La Mar, T. Li, G.N.J. Phillips, R.F. Eich, J.S. Olson, J. Ling, D.F. Bocian, A double mutant of sperm whale myoglobin mimics the structure and function of elephant myoglobin, J. Biol. Chem. 270 (1995) 20763–20774.

[36] J.M. Kriegl, A.J. Bhattacharyya, K. Nienhaus, P. Deng, O. Minkow, G.U. Nienhaus, Ligand binding and protein dynamics in neuroglobin, Proc. Natl. Acad. Sci. U. S. A. 99 (2002) 7992–7997.

[37] P.K. Gupta, Dynamic range problem in Fourier transform NMR. Modified WEFT pulse sequence, J. Magn. Reson. 24 (1976) 461–465.

[38] J. Jeener, B.H. Meier, P. Bachmann, R.R. Ernst, Investigation of exchange processes by two-dimensional NMR spectroscopy, J. Chem. Phys. 71 (1979) 4546–4553.

[39] C. Griesinger, G. Otting, K. Wuthrich, R.R. Ernst, Clean TOCSY for proton spin system identification in macromolecules, J. Am. Chem. Soc. 110 (1988) 7870–7872.

[40] Z.C. Xia, B. Nguyen, G.N. La Mar, The use of chemical shift temperature gradients to establish the paramagnetic susceptibility tensor orientation: implication for structure determination/refinement in paramagnetic metalloproteins, J. Biomol. NMR 17 (2000) 167–174.

[41] K. Rajarathnam, G.N. La Mar, M.L. Chiu, S.G. Sligar, Determination of the orientation of the magnetic axes of the cyano-MetMb complexes of point mutants of myoglobin by solution ^{1}H NMR: influence of His(E7)Gly and Arg(CD3)Gly substitutions, J. Am. Chem. Soc. 114 (1992) 9048–9058.

[42] A. Bundi, K. Wuthrich, ^{1}H-NMR parameters of the common amino acid residues measured in aqueous solutions of the linear tetrapeptides H-Gly-Gly-X-L-Ala-OH, Biopolymers 18 (1979) 285–297.

[43] D.S. Wishart, B.D. Sykes, F.M. Richard, Relationship between nuclear magnetic resonance chemical shift and protein secondary structure, J. Mol. Biol. 222 (1991) 311–333.

[44] K.J. Cross, P.E. Wright, Calibration of ring-current models for the heme ring, J. Magn. Reson. 64 (1985) 231–240.

[45] S.D. Emerson, G.N. La Mar, NMR determination of the orientation of the magnetic susceptibility tensor in cyanometmyoglobin: a new probe of steric tilt of bound ligand, Biochemistry 29 (1990) 1556–1566.

[46] P. Ferrara, H. Gohlke, D.J. Price, G. Klebe, C.L. Brooks, Assessing scoring functions for protein–ligand interactions, J. Med. Chem. 47 (2004) 3032–3047.

[47] J. Qin, G.N. La Mar, F. Ascoli, M. Brunori, Solution NMR determination of active site structure for a paramagnetic protein: cyano-met *Aplysia* Mb, J. Mol. Biol. 231 (1993) 1009–1023.

[48] Z.C. Xia, D.N.Y. Bao, M. Brunori, F. Cutruzzola, G.N. La Mar, H-1-NMR study of the effect of temperature through reversible unfolding on the heme pocket molecular structure and magnetic properties of *Aplysia limacina* cyano-metmyoglobin, Biophys. J. 89 (2005) 4149–4158.

[49] K. Nienhaus, A. Ostermann, G.U. Nienhaus, F.G. Parak, M. Schmidt, Ligand migration and protein fluctuations in myoglobin mutant L29W, Biochemistry 44 (2005) 5095–5105.

[50] K. Wüthrich, NMR of Proteins and Nucleic Acids, John Wiley & Sons, New York, 1986.

[51] J. Qin, G.N. La Mar, Complete sequence-specific assignment of hyperfine-shifted residues in the active site of a paramagnetic protein: cyano-met *Aplysia* myoglobin, J. Biomol. NMR 2 (1992) 597–618.

[52] K. Rajarathnam, J. Qin, G.N. La Mar, M.L. Chiu, S.G. Sligar, Solution structure determination of the heme cavity in the His (E7)Val cyano-met myoglobin point mutant based on the proton NMR detected dipolar field of the iron: evidence for contraction of the heme pocket, Biochemistry 32 (1993) 5670–5680.

[53] G.N. La Mar, J.D. Satterlee, J.S. de Ropp, in: K.M. Kadish, R. Guilard, K.M. Smith (Eds.), The Porphyrins Handbook, Academic Press, San Diego, USA, 1999, pp. 185–298.

[54] B.D. Nguyen, Z.C. Xia, D.C. Yeh, K. Vyas, H. Deaguero, G.N. La Mar, Solution NMR determination of the anisotropy and orientation of the paramagnetic susceptibility tensor as a function of temperature for metmyoglobin cyanide: implications for the population of excited electronic states, J. Am. Chem. Soc. 121 (1999) 208–217.

[55] W.H. Du, Z.C. Xia, S. Dewilde, L. Moens, G.N. La Mar, ^{1}H NMR study of the molecular structure and magnetic properties of the active site for the cyanomet complex of O_2-avid hemoglobin from the trematode *Paramphistomum epiclitum*, Eur. J. Biochem. 270 (2003) 2707–2720.

[56] F.A. Walker, The heme environment of mouse neuroglobin: histidine imidazole plane orientations obtained from solution NMR and EPR spectroscopy as compared with X-ray crystallography, J. Biol. Inorg. Chem. 11 (2006) 391–397.

[57] V. Bondarenko, S. Dewilde, L. Moens, G.N. La Mar, Solution ^{1}H NMR characterization of the axial bonding of the two his in oxidized human cytoglobin, J. Am. Chem. Soc. 128 (2006) 12988–12999.

[58] H. Sawai, M. Makino, Y. Mizutani, T. Ohta, H. Sugimoto, T. Uno, N. Kawada, K. Yoshizato, T. Kitagawa, Y. Shiro, Structural characterization of the proximal and distal histidine environment of cytoglobin and neuroglobin, Biochemistry 44 (2005) 13257–13265.

[59] S. Fordel, L. Thijs, L. Moens, S. Dewilde, Neuroglobin and cytoglobin expression in mice, FEBS J. 274 (2007) 1312–1317.